


A simple atomization approach enables monolayer dispersion of nano graphenes in cementitious composites with excellent strength gains

Journal Article

Author(s):

Dang, Nanxi; Yang, Rijiao; Xu, Chengji; Peng, Yu; Zeng, Qiang; Zhao, Weijian; [Zhang, Zhidong](#) 

Publication date:

2023

Permanent link:

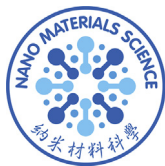
<https://doi.org/10.3929/ethz-b-000638179>

Rights / license:

[Creative Commons Attribution-NonCommercial-NoDerivatives 4.0 International](#)

Originally published in:

Nano Materials Science, <https://doi.org/10.1016/j.nanoms.2023.09.004>



Contents lists available at ScienceDirect

Nano Materials Science

journal homepage: www.keaipublishing.com/cn/journals/nano-materials-science/

A simple atomization approach enables monolayer dispersion of nano graphenes in cementitious composites with excellent strength gains

Nanxi Dang^{a,b}, Rijiao Yang^a, Chengji Xu^{a,c}, Yu Peng^a, Qiang Zeng^{a,**}, Weijian Zhao^{a,*}, Zhidong Zhang^d^a College of Civil Engineering and Architecture, Zhejiang University, 310058, Hangzhou, China^b Center for Balance Architecture, Zhejiang University, Hangzhou, 310028, China^c The Architectural Design & Research Institute of Zhejiang University Co., Ltd, Hangzhou, 310063, China^d Institute for Building Materials, ETH Zurich, 8093, Zurich, Switzerland

ARTICLE INFO

Keywords:

Nanomaterials
Dispersion
Atomization
Strength
Microstructure

ABSTRACT

Carbon nano additives (CNAs) are critical to achieving the unique properties of functionalized composites, however, controlling the dispersion of CNAs in material matrix is always a challenging task. In this study, a simple atomization approach was successfully developed to promote the dispersion efficiency of graphene nanoplatelets (GNPs) in cement composites. This atomization approach can be integrated with the direct, indirect and combined ultrasonic stirrings in a homemade automatic stirring-atomization device. Mechanical and microstructure tests were performed on hardened cement pastes blended with GNPs in different stirring and mixing approaches. Results show that the direct ultrasonic stirrings enabled more homogeneous dispersions of GNP particles with a smaller size for a longer duration. The atomized droplets with the mean size of $\sim 100 \mu\text{m}$ largely mitigated GNPs' agglomerations. Monolayer GNPs were observed in the cement matrix with the strength gain by up to 54%, and the total porosity decrease by 21% in 0.3 wt% GNPs dosage. The greatly enhanced dispersion efficiency of GNPs in cement also raised the cement hydration. This work provides an effective and manpower saving technique toward dispersing CNAs in engineering materials with great industrialization prospects.

1. Introduction

Embedding carbon nano additives (CNAs) into material matrix is an effective approach to developing novel composites with excellent performances, such as long durability, high strength, and enhanced electrical properties [1,2]. Graphene nanoplatelets (GNPs), an important family member of CNAs, possess various extraordinary properties, e.g., low density, high toughness strength and flexibility, and excellent electrical conductivity [3–5], and have been extensively employed to develop functional materials [6–9]. As to cementitious materials (CMs), the most used manmade construction materials worldwide [10,11], the addition of appropriate dosages of GNPs into cement matrix can have significant impacts on the micro-structure, mechanical properties and durability of CMs [12,13]. Literature survey indicates that CMs with GNPs demonstrated compressive strength promotions by about 8–38% [14–19]. However, the difficulties and diversities in dispersion of GNPs would greatly limit the applications of GNPs in engineering practices [20].

Therefore, developing an efficient and robust dispersion method is urgently needed before the large-scale applications of GNPs in the construction industry.

Due to the high specific surface area (SSA) and surface energy of GNPs, the attraction of GNP particles can easily lead to agglomerations [21,22], which may act as the defects in the matrix and consequently decrease the engineering properties of CMs [23,24]. The formation of GNP agglomerations mainly includes two main mechanisms: (1) face-to-face interactions, where some functional groups such as hydroxyl and epoxy groups adsorbed on the surface of GNPs can form hydrogen bonds with divalent cations between GNP layers; and (2) edge-to-edge interactions, where carboxylic acid groups at the edge of GNPs bridge the surrounding GNP sheets through complexation reaction [25,26]. To reduce the physical and chemical interactions between GNPs, chemical dispersants, such as polycarboxylate (PCE) superplasticizer [27,28], naphthalenesulfonate (NS) superplasticizer [29], Gum Arabic [30,31], sodium dodecyl sulfate [32,33] and polyether amine [34], have been

* Corresponding author.

** Corresponding author.

E-mail addresses: cengq14@zju.edu.cn (Q. Zeng), WeijianZhao@zju.edu.cn (W. Zhao).<https://doi.org/10.1016/j.nanoms.2023.09.004>

Available online xxx

2589-9651/© 2023 Chongqing University. Publishing services by Elsevier B.V. on behalf of KeAi Communications Co. Ltd. This is an open access article under the CC BY-NC-ND license (<http://creativecommons.org/licenses/by-nc-nd/4.0/>).

developed. For example, the most widely used PCE dispersant enables negative charges on CNAs, thereby generating electrostatic repulsion and promoting dispersion [35]. An experimental study [36] suggested that melamine may possess the higher dispersion efficiency and stabilization on the exfoliated GNPs suspension than other dispersants.

Meanwhile, for most studies, physical (or mechanical) dispersion methods including electromagnetic stirrings and ultrasonic stirrings [37–39] are often used in combination with chemical dispersants towards better dispersion of GNPs and other CNAs. Through transmitting and generating pressure waves in aqueous that lead to the formation and collapse of microscopic bubbles (cavitation), ultrasonic stirring can break up the agglomerations of nano particles [40]. Key parameters of ultrasonic dispersion include frequency, power input, duration, type of ultrasound and temperature [41]. It has shown that dispersion uniformity and stability are proportional to sonication time within 2 h [41–43]. However, a long-time stirring of bath ultrasonic may lead to an unfavorable increase in temperature of the suspension [44]. Compared with ultrasonic bath, direct ultrasonic (DU) stirrings with ultrasonic probe showed a higher dispersion efficiency [45].

While the dispersion of GNP suspensions has attracted great attention, the subsequent mixing, however, has been relatively less investigated. For CMs with GNPs and other nanomaterials, several mixing methods have been developed [46–49]. Generally, the well-dispersed GNP suspensions are added to the dry-mixed cement powder, then an ordinary mechanical mixing scheme is performed to obtain cement slurries [50]. In some cases, all the dry materials (including the GNPs and cement) are first mixed, then water and superplasticizer are added to the dry-mixed materials followed by the mechanical mixing. To enhance the homogeneity of nanoparticles in cement slurries, some further mixing methods, such as, high-speed shear mixer [51,52], addition of carrier (e.g., silica fume), and ball milling approach [53,54], have been developed.

Even so, it is still difficult to achieve a sufficient and uniform mixing system of cement slurries containing GNPs as well as other nanomaterials. Furthermore, GNPs may further agglomerate together with cement hydration. When GNPs are exposed to a high pH environment (such as cement solution), the hydrophilicity of GNPs decreases due to the reduction of some functional groups [55], which may enhance the agglomerations of GNPs. It is worth noting that the aggregated GNPs in alkaline cement paste could not be completely avoided because of the appearance of rich calcium cations. At present, the sprayable engineered method has been widely used in preparing cement composites, especially in repair materials, green environmental protection materials and plastic materials [56–58]. Hartono et al. [59] investigated the effectiveness of dry and spray pulverized method on cement-stabilized clay shale and sandstone and the spray-pulverized process generated specimens with more toughness than the dry pulverized method. Li et al. [60] compared different nano-silica (NS) treatment methods, namely pre-spraying and pre-mixing, and proved that the specimens prepared by the pre-spraying method showing superior performance could be ascribed to the better enhanced interfacial transition zone.

Note that, due to the large specific surface areas, CNAs remains still easy to agglomerate and the spraying methods still cannot avoid the agglomerations [61,62]. However, if the sprayable liquid can be separated to extremely fine droplets, dispersion would be further enhanced. Atomization can be used to break up a liquid into small droplets with the size between 10 μm and 1000 μm [63]. Inspired by those findings, we propose that a better dispersion may be achieved by a simply atomizing technique. Furthermore, there is almost no integrated method that can efficiently and robustly disperse nanomaterials in CMs and other engineering materials. Here, we seek to develop an atomization mixing scheme integrated with ultrasonic stirrings to avoid the mutual contact of adjacent GNP sheets in the matrix of CMs. This work is organized as follows: first, the materials and experimental methods are present; later, the dispersion efficiencies of GNPs in water and cement solution with the

indirect, direct and combined ultrasonic stirrings (named IU, DU and IDU, respectively) are compared; after that, the mechanical properties, microstructure, and chemical characteristics of hardened cement pastes (HCPs) prepared with different stirring and mixing methods are investigated; finally, the main conclusions of this work are summarized.

2. Materials and methods

2.1. Materials

GNP powder (purity >99.5%) was purchased from XFANO Materials Co., Ltd (Nanjing, China). Melamine was used as the chemical dispersant (MELMENT@F10, BASF Co., Ltd. Germany) according to our previous work [36]. A Portland cement P-I (identical to ASTM type I) was used as the only binder for preparing the HCP samples (more information of GNPs and cement used in this study can be found in the supporting information, Tables S1 and S2 and Fig. S1).

2.2. Experimental procedures

2.2.1. Preparation of GNP suspensions

To prepare a stably dispersed GNP suspension, the precisely weighed Melamine dispersant was first dissolved in water in a beaker by hand stirrings to achieve the complete dissolution of the dispersant, then GNPs were put into the beaker carefully. After that, the GNP suspensions experienced three different stirring methods: IU, DU and IDU. For IU, bottles filled with GNP suspensions were put in the ultrasonic vibrating pot (Jiekang PS-20, 120W) filled with water, while for DU, the tip ultrasonicator (Jiekang CE-9600, 70W) was directly put in GNP suspensions (Fig. 1). The stirring duration of 2 h was used for both IU and DU, while for IDU, the GNP suspensions experienced both IU and DU for 1 h.

Noted that although GNPs can be dispersed in water, they immediately agglomerate together in alkaline cement pore solution (CPS), since the large number of divalent ions, such as Ca^{2+} , can cross-link the single layer of GNP into multi-layers and turn them to much larger dimensions [37,38]. To understand the possible influences of CPS, two different suspensions were prepared: distilled water and cement solution. Therefore, the sample ID of this work was designed as dispersion methods + liquid media. For example, D0 and DC, respectively, represent the GNP suspensions dispersed in water (tail symbol of 0) and cement pore solution (tail symbol of C) with direct ultrasonic stirring. The mixing proportions are presented in Table 1.

2.2.2. Mix design and specimen preparation

To achieve a better mixing of the GNP suspensions and cement, an atomization mixing method was introduced. A nano-atomizer was fixed on the ultrasonic device to develop a home-made integrated stirring-atomization device (Fig. 1). Through this device, GNP suspensions can be automatically atomized into cement. The water-to-cement (w/c) ratio for all mixes was 0.35. Specimens were designed and labeled as mixing method + dispersion method (Table 2). For example, D-I indicates direct mixing + indirect ultrasonic stirring. The mixing proportions (six levels of GNPs contents, namely, 0, 0.05%, 0.1%, 0.3%, 0.5% and 1% by cement weight) for all cement pastes are presented in Table 3. The dosages of dispersant are consistent with that of GNPs.

The cement pastes were prepared as follows. First, the readily prepared GNP suspensions were mixed with cement powder for 5 min. Two traditional mixing methods and the proposed hybrid ultrasonic stirring and atomization mixing approach were used to prepare the cement slurries with GNPs (Fig. 1). The fresh cement pastes were immediately poured into cubic molds with the dimensions of $20 \times 20 \times 20 \text{ mm}^3$ and vibrated for 2 min. After 24 h, the cement paste cubes were demolded and cured in a chamber with standard curing conditions (temperature of $20 \pm 2 \text{ }^\circ\text{C}$ and relative humidity >95%) for 27 d.

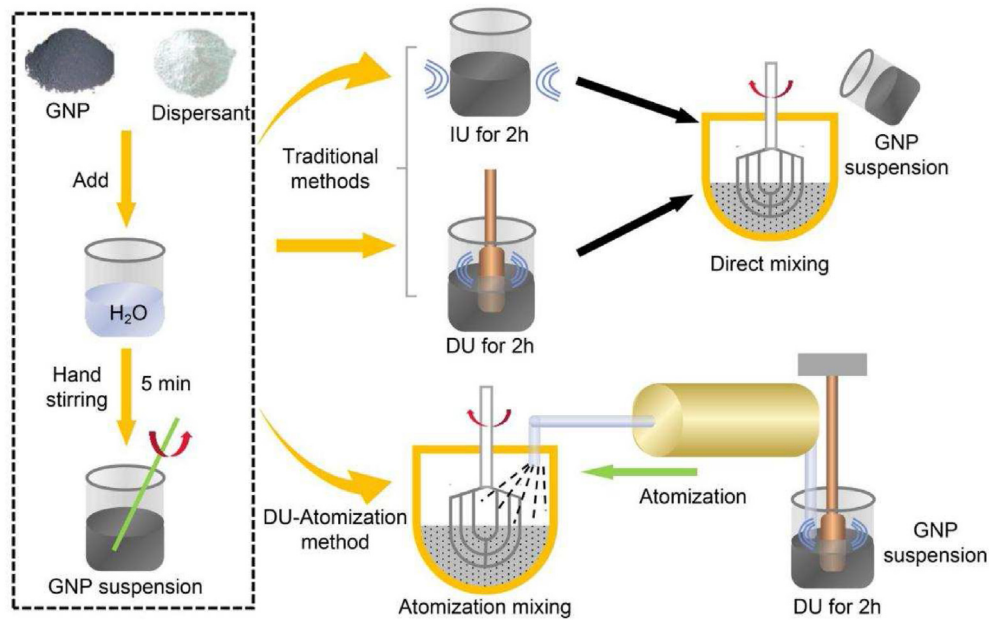


Fig. 1. Preparations of cement slurries with GNPs by the DU, IU and hybrid ultrasonic stirring and atomization mixing strategy.

Table 1

Sample ID of GNP suspensions with different stirrings.

Sample	Stirring	Water (g)	Dispersant (g)	GNPs (g)	Cement (g)
IO	IU(2h)	100	1	1	0
IDO	IDU (IU for 1h + DU for 1h)				
D0	DU(2h)				
IC	IU(2h)				4
IDC	IDU (IU for 1h + DU for 1h)				
DC	DU(2h)				

Table 2

Mixing and stirring methods used in this work.

Sample	Mixing method	Stirring
D-I	Direct mixing	IU(2h)
D-ID		IDU (IU for 1h + DU for 1h)
D-D		DU(2h)
A-I	Atomization mixing	IU(2h)
A-ID		IDU (IU for 1h + DU for 1h)
A-D		DU(2h)

Table 3

Mix proportions of the cementitious composites.

GNP content (wt %)	GNPs (g)	Dispersant (g)	w/c	Cement (g)	Water (g)
0	0	0	0.35	300	105
0.05	0.15	0.15			
0.1	0.3	0.3			
0.3	0.9	0.9			
0.5	1.5	1.5			
1.0	3.0	3.0			

2.3. Test methods

2.3.1. Particle size analysis

A laser particle size analyzer (Coulter LS13320, America) and an optical microscope (CX40 M Shunyu, Ningbo, China) were used to measure

the GNP particle size. The refractive index for the laser particle size analyzer was 1.333. For visual rating, 50 ml of each GNP suspension after three ultrasonic stirring schemes were placed in tubes to examine the possible sedimentation by the eyes per hour. After 4 h, the upper, middle and lower GNP suspensions were removed on slide glasses with rubber droppers, and massive microscopic pictures were acquired by the optical microscope at different magnifications [64]. For microscopic imaging analysis, particle size distribution (PSD) was quantitatively analyzed by the software of Image Pro Plus 6.0. The Gaussian blur threshold was employed to identify the GNP clusters. Thereafter, the average particle size of each selected area was calculated.

2.3.2. UV-visible tests

UV-Vis analysis was carried out to determine the absorbance of different suspensions. The GNP suspensions were first diluted 50 times and the distilled water was used to preset the zero absorbance of the reference medium before tests. A UV-Vis spectroscopy (UV-2600, Shimadzu, Guangzhou, China) was operated at 190 to 900 nm range. To measure the absorbance of the suspensions with the elapsed time after the completion of ultrasonic dispersion, only the incident light with the wavelength of 600 nm was chosen, the absorbance of each suspension was measured every 5 min at 600 nm, and lasted for 20 min.

2.3.3. Mechanical strength

Compression tests were carried out via a 250 kN Instron hydraulic testing machine (Type 8802, Instron, USA). After curing for 27 d under standard curing conditions, six groups of the HCP specimens with GNPs of $2 \times 2 \times 2$ cm³ prepared by different dispersion methods were tested to evaluate the best stirring and mixing protocol. Under the optimal dispersion, the six groups of GNPs contents by cement weight in Table 3 were also used to test the effect of GNP concentration on compressive strength after a standard curing. A force control mode was applied to raise forces at the speed of 35 kN/min until the load dropped by 50%.

2.3.4. Scanning electron microscopy

Samples for SEM tests were prepared from the crushed segments after compression tests. A FEI Quanta FEG 650 ESEM with the accelerating voltage of 20 keV and spot size of 4.0 was applied to characterize the micro morphology of the HCP samples. All the segments were cut into small pieces without surface polishing to keep the original morphology.

After oven-drying, a plasma spraying process was used to coat a gold film on each sample. Then the samples were placed in a vacuum environment to observe the surface.

2.3.5. X-ray computed tomography

A device of XTH 255/320 LC (NIKON, Japan) equipped with a high-resolution detector (2000×2000 pixels) was used to perform X-ray scans. Small cubes in the dimensions of $10 \times 10 \times 20 \text{ mm}^3$ acquired from the large GNP-modified cement composites were prepared for the XCT test. To improve the XCT testing efficiency, 3 samples were stacked up as one large sample for X-ray scans. After the samples were fixed on the sample frame, it rotated at a speed of $12^\circ/\text{min}$ for X-ray penetration. The X-ray beam was generated at an accelerating voltage of 100 kV and a beam current of 80 μA . A Cu film with a thickness of 0.25 mm was attached to the X-ray emission tube to filter out the low-energy X-rays. The exposure time of each image was 0.72 s, and a complete scan would generate a total of 2500 images. The images were reconstructed by the software of VG Studio Max 3.1. The typical pixel resolution of the XCT tests was 6.7 μm . Because the attenuations of materials depend on the interaction between X-rays and the components [65], it is possible to resolve the 3D structure of GNP agglomerations in cement matrix.

2.3.6. Mercury intrusion porosimetry

Small HCP segments ($10 \times 10 \times 10 \text{ mm}^3$) cut from cast cubes were adopted for mercury intrusion porosimetry (MIP) tests in a device of Autopore IV 9510 (Micromeritics Instrument Corporation, USA). The intrusion pressure was performed progressively from 0.5 psi to 60000 psi with an equilibrium time of 10 s. The surface tension of mercury and the mercury-pore wall contact angle were assumed as 0.485 N/m and 130° , respectively. According to the Washburn equation, the minimum and maximum pore sizes of around 3 nm and 360 μm were obtained [66].

2.3.7. Chemical tests

Powder samples with a size smaller than 75 μm were milled for chemical tests. TG/DTG tests were conducted in an apparatus of TGA/DSC3+ (ETTLER TOLEDO, Switzerland). During testing, the cement powders ($\sim 10 \text{ mg}$) were loaded in the alumina crucible of the device, later, the rise of temperature from 50°C to 1000°C at the rate of $10^\circ\text{C}/\text{min}$ was set to heat the sample. To preserve the possible contamination of the sample by the air, a nitrogen flow of 100 ml/min was applied.

FTIR tests were conducted in a device of Nicolet5700 (Thermo Fisher Scientific Co., USA). Free-sample FTIR scans ran before formal tests to filtrate possible noise signals. Later, the HCP samples were scanned by the FTIR device from 4000 to 400 cm^{-1} in the resolution of 2 cm^{-1} .

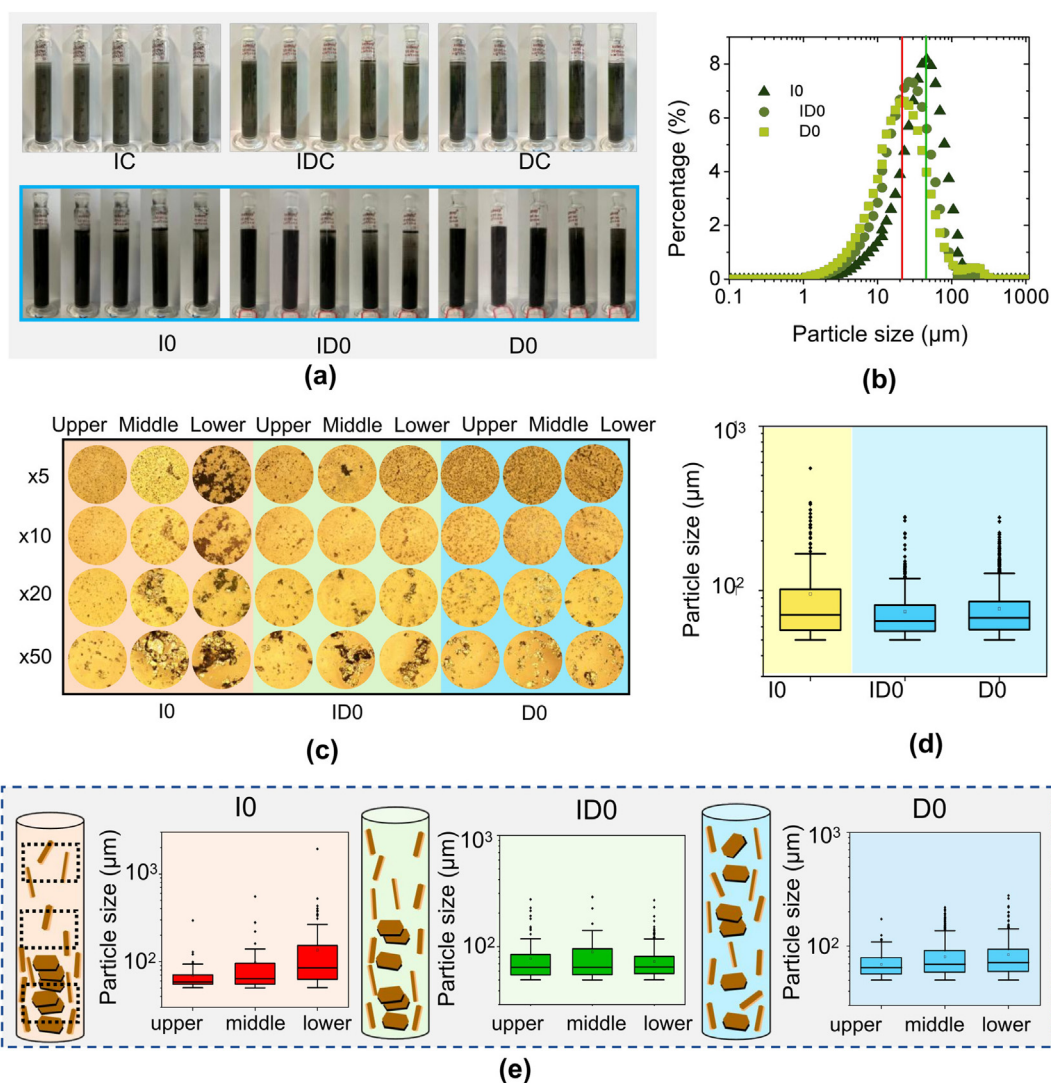


Fig. 2. Dispersion of GNPs in water and cement solution: (a) sedimentation of GNPs in different suspensions prepared by three stirring methods, (b) PSD curve of I0, ID0 and D0, (c) microscopic images of GNP suspensions at different magnifications, (d) statistic particle sizes of GNPs, and (e) particle sizes of GNPs in the upper, middle, and lower layers of I0, ID0 and D0 samples.

XRD tests were performed using the equipment of Bruker (Germany) D8 ADVANCE X-Ray diffractometer. The goniometer speed of $0.02^\circ/\text{s}$ was chosen in the scattering ranges from 5° to 70° . The X-ray source used was the K- α line of copper radiation ($k = 1.54056 \text{ \AA}$). Peaks of the minerals present in the sample have been identified using the software of Jade 6.0.

3. Results and discussion

3.1. GNP dispersion

Fig. 2a shows the typical images of GNP sedimentation in different suspensions with three stirring schemes. The settlement of GNP suspensions was photographed and recorded per hour. The dispersion efficiency of different stirring methods was determined by observing the color of suspension and GNP sedimentation. Samples I0 and ID0 showed a lighter color near the floats upon the suspension, but a darker color near the bottom. For sample D0, even after 4 h' settlement, the color of the suspension was uniform, which suggests that the GNPs have been stably and homogeneously dispersed in the solution. Moreover, the precipitations of GNP particles in the cement solution were essentially severer than those in the distilled water (Fig. 2a). Those testified that the presents of ions dissolved from cement clinkers may break the balance of complex physical and (electro)chemical interactions between GNPs, which therefore deteriorates the dispersion stability [27].

In the PSD diagram (Fig. 2b), the peak size of I0 was $44 \mu\text{m}$ while that of D0 was $21 \mu\text{m}$. This indicates that the GNP sedimentation in D0 (direct ultrasonic stirrings) was less than I0 (indirect ultrasonic stirrings). The stability and uniformity of GNPs in water stirred by three stirring methods were further evaluated through optical microscopic observation

and imaging analysis. The upper, middle and lower layers of the GNP suspensions after 4-h's sedimentation were dropped on a glass slide to conduct microscopic observation. Fig. 2c shows the images with different magnifications ($\times 50$, $\times 20$, $\times 10$ and $\times 5$). The black part with metallic luster in the pictures represents GNP particles. The upper, middle and lower layers of I0 possessed different characteristics than those of ID0 and D0. Fewer GNPs were observed in the upper layer while a large number of GNPs precipitated in the lower layer. The agglomeration of GNPs can be observed at higher magnifications, indicating that after ultrasonication, there were still severe GNP agglomerations in the suspension. For ID0, the reduction of graphene sheets in the lower layer can be observed ($\times 5$), but some large GNP agglomerations were observed under a higher magnification ($\times 50$). For D0, it can be observed that the size and distribution of GNPs in the upper, middle and lower layers did not show much difference under $\times 5$, indicating that the DU method can effectively improve the uniformity and stability of GNP dispersion in an aqueous solution [36,67].

Fig. 2d shows the statistic plots of GNPs' PSD under different stirring methods. Clearly, the GNPs' particle sizes of ID0 and D0 were smaller than that of I0. Fig. 2e shows the results of GNPs' particle size on the upper, middle and lower layers of each sample. Clearly, for I0, the large GNP particle size differences could be observed among the layers, indicating severe agglomerations and sedimentation [42,68]. For the I0 upper layer solution, the particles below $100 \mu\text{m}$ accounted for 98%, while in the middle and lower layers, they decreased by 7% and 14%, respectively. The maximum particle size of the lower layer solution was $532 \mu\text{m}$. For the upper solution of ID0, the particles below 100 accounted for 91%, and the differences from those in the middle layer and the lower layer were 10% and 3%, respectively. The maximum particle size of the lower solution was $261 \mu\text{m}$. For the top solution of D0, the proportion of

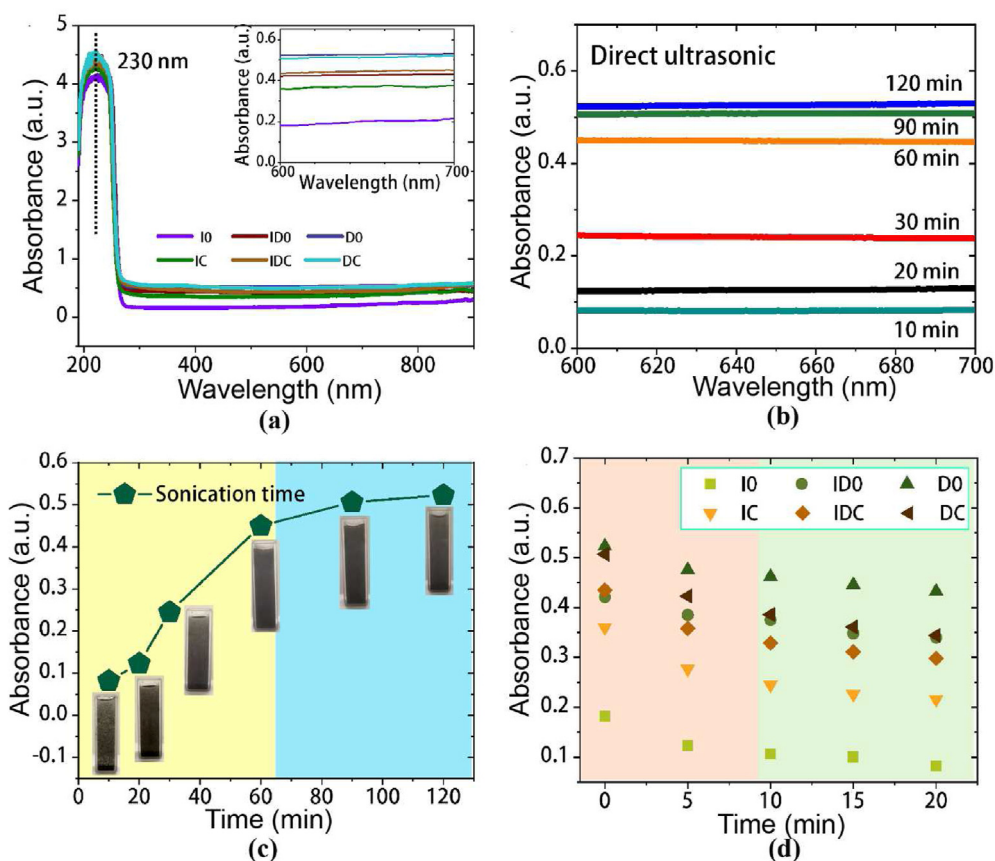


Fig. 3. UV-Vis data: (a) absorbance spectra of GNP suspensions prepared by different stirring methods under the ultraviolet wavelength of 190-900 and 600-700 nm (inset panel), (b) absorbance of GNP suspension after DU treatment under the ultraviolet wavelength of 600-700 nm, (c) absorbance of GNP suspension after different ultrasonic time under the ultraviolet wavelength of 600 nm, (d) absorbance spectra of GNP suspensions under different sedimentation time.

the particles smaller than 100 μm was 99%, and the differences from the middle and lower layers showed the particle size differences by 9% and 14% respectively. The maximum particle size of the lower layer solution was 278 μm . The results indicate that DU would significantly improve the dispersion efficiency of GNPs in water.

Fig. 3a shows the absorbance spectra of GNP suspensions with and without cement prepared by different ultrasonic stirring methods (I0, ID0, D0, IC, IDC and DC). It can be observed that the spectra of all the suspensions showed a rapid increase in absorbance up to 230 nm, corresponding to the carbon structure in carbon nanomaterials [69]. The wavelength region with stable absorption spectrum (600 nm to 700 nm) was selected to compare the absorbance of six groups of samples. Generally, a higher absorbance means a better dispersion of different suspensions, because the agglomerated and precipitated particles in segregated suspensions have poor performance to absorb light. Therefore, the data of Fig. 3a again evidenced the augmentation of the uniformity and stability of GNPs in liquid with DU.

To study the effect of ultrasonic time on the dispersion of GNP suspension, different ultrasonic durations (10, 20, 30, 60, 90 and 120 min) were set for the DU method (Fig. 3b and c). Fig. 3b shows that the absorbance of GNP suspension after the DU treatment increased with the increase of sonication time. The changes of the absorbance at a wavelength of 600 nm with ultrasonic time and the images of the GNP suspensions are shown in Fig. 3c. During the first 60 min, the absorbance gradually increased with the increase of sonication time by 0.37. Within 60-120 min, the absorbance increased by 0.073. The observations indicate that the sonication time affected the uniformity of GNP dispersion in solution in the first 60 min. The findings are in good agreement with the data reported in the literature [41,70].

Fig. 3d shows the absorbance spectra of GNP suspensions under different sedimentation time. It was observed that the absorbance of all GNP suspensions at the beginning of measurement decreased with time because of agglomerations of the GNP particles. For example, the absorbance of I0 decreased by 0.076 in 0-10 min and 0.024 in 10-20 min. As for D0, the absorbance decreased by 0.061 in 0-10 min and 0.029 in

10-20 min. It seems that the cement pore solution would cause a faster decrease of the absorbance with time. For example, the sample of DC showed a rapid decrease of absorbance from 0.51 to 0.35 in 20 min (Fig. 3d). This evidenced that the CPS can enhance the agglomeration of carbon nanoparticles [55].

3.2. Atomization characteristics

The atomization process enables generating extremely fine liquid drops containing GNP particles. Due to the small size of the atomized droplets, the agglomeration of GNPs should be greatly mitigated. To clarify the mechanisms of the improved GNP dispersion, the nano-atomized droplets were measured (Fig. 4a). Microscopic images showed that over 90% of the droplets had the size less than 300 μm , and 55% of them were between 50 and 150 μm . Statistic results displayed that the atomization allowed formation of small droplets with the average size of $\sim 100 \mu\text{m}$ that contain GNPs (Fig. 4a). In this condition, the GNPs cannot be larger than the droplets, so the GNPs' agglomerations were greatly avoided.

The dispersion of GNP sheets in the dry cement particles and hardened cement paste was illustrated in Fig. 4b based on the main findings discussed above. During the atomization mixing, the significant agglomerations of GNP sheets were avoided due to the atomization. Meanwhile, the oxygen functional groups exposed on the basal plane and on the edges of the nanosheets may further separate them [71]. Parceling GNP sheets in droplets and mixing them with cement particles not only have benefits to the dispersion of GNPs, but also improve the physical attachment of GNPs on cement particles during mixing. As a result, GNPs can be successfully isolated by the cement particles to achieve enhanced dispersion in the dry cement matrix. At the macro scale, those GNPs may act as reinforcements, so the compressive strength can be greatly raised; at the micro scale, the functional groups on the surface of GNP sheets would yield the stronger interactions with cement hydrates. Detailed discussions are presented in the following sections.

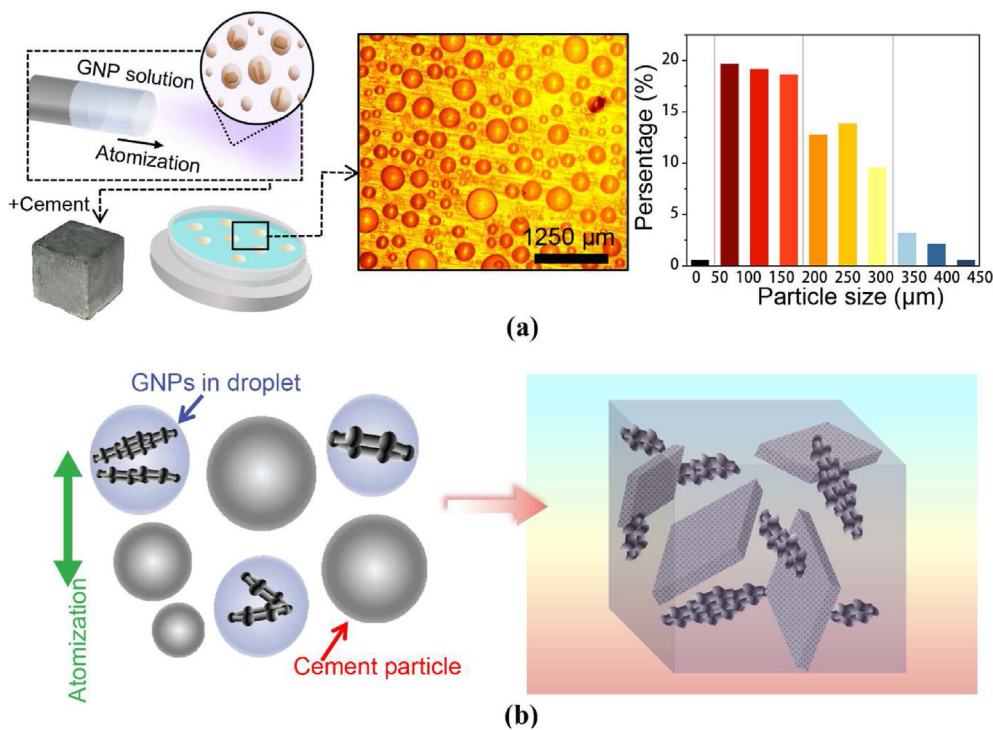


Fig. 4. Mechanisms of GNP dispersion with atomization: (a) schematic illustration of atomizing process (left), a selected microscopic picture of the atomized droplets (middle), and PSD of the atomized droplets (right), (b) schematic demonstration of the dispersion of droplets with GNPs in dry cement particles and hardened cement paste.

3.3. Compression strength

Fig. 5a displays the stress-strain curves of HCP composites with six different GNP contents (0%, 0.05%, 0.1%, 0.3%, 0.5% and 1.0%) under the hybrid ultrasonic stirring and atomization mixing (A-D group). The stress-strain curves showed similar shapes, suggesting that all the materials followed the same failure mechanisms under the compression loads. The peak strength was identified as compressive strength. It increased first and then decreased with increasing the GNP content. Specifically, as the GNP dosage increased from 0 to 0.3%, and to 1%, the compressive strength increased from 54.2 MPa to 83.5 MPa (by 54%), but decreased slightly to 54.1 MPa. The sample with 0.3% GNPs showed the highest compressive strength. This result was consistent with the data documented elsewhere [36].

The compressive strength and relative improvement of six CM groups (with 0.3% GNPs) compared with the blank one (0% GNPs) are shown in Fig. 5b and c. Clearly, all the CM samples with 0.3% GNPs possessed promotions in compressive strength in different extents. In addition, further characteristics can be observed. First, the strength of the GNP-modified CMs prepared by the atomization mixing was significantly higher than those prepared by the ordinary mixing method. Second, apparently, the increase of the DU duration promoted the compressive strength for both the traditional and atomization mixing methods (Fig. 5b). Our data showed the A-D sample had the highest compressive strength up to 83.5 MPa, 54% higher than the reference one (Fig. 5c). Fig. 5d compared the relative strength enhancements of GNP-modified CMs in this work and other studies [15,17,20,25,26]. It can be found that the average compressive strength promotion was approaching 10%, while our optimal sample was almost 5 times higher. The data indeed

evidenced that the hybrid DU and atomization approach can greatly improve the compressive strength of cement composites with GNPs.

3.4. Micro morphology

SEM images of the GNP-modified cement composites with the fabrication methods of D-I, D-ID, D-D, A-I, A-ID and A-D are selectively displayed in Fig. 6. Clearly, the traditional direct mixing method would cause the wrinkled agglomerations of GNPs in the cement matrix (samples D-I and D-ID; see Fig. 6a and b). The longtime direct ultrasonic dispersion mitigated the agglomerations (sample D-D; see Fig. 6c).

When the atomization mixing was used, small agglomerations with several layers of GNP emerged in sample A-I (Fig. 6d), and mono-layered GNPs can be observed in samples A-ID and A-D (Fig. 6e and f). It can be figured out that the graphene sheets in the A-D sample were much smaller than those observed in other cases. The monolayer dispersion of thin graphene nanosheets in cement matrix certainly accounted for the greatest strength gains as observed in Fig. 5. Based on the data of mechanical properties (Fig. 5) and micro morphology (Fig. 6), the specific GNP agglomerations, pore structure and chemical analyses were conducted to the samples A-D and D-I, respectively, for comparison.

3.5. Characterization of agglomerations

GNP agglomerations and large pores (and/or air voids) in the GNP-modified CMs (samples A-D and D-I) were characterized by XCT (Fig. 7a). Generally, the gray values of XCT images are sensitive to the density of the phase tested, therefore, GNPs and pores with low densities can be identified accordingly [65]. As an example, Fig. 7b illustrates the

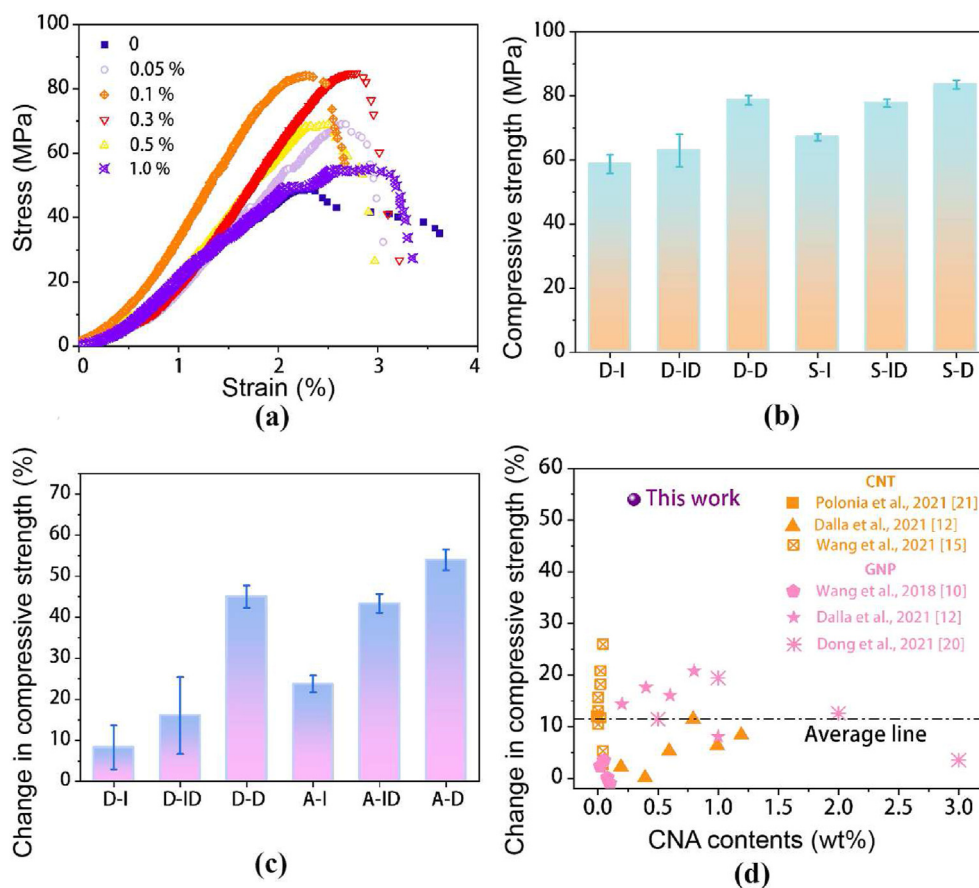


Fig. 5. Mechanical properties of nano engineered CM: (a) Compressive stress-strain curves of the HCPs with GNPs at different dosages (0, 0.05%, 0.1%, 0.3%, 0.5% and 1.0%) with the A-D approach, (b) compressive strength of six HCP groups, (c) percentage increase of compressive strength relative to the sample without GNP, (d) comparison of strength rise ratio between our data and those in the literature [15,17,20,25,26].

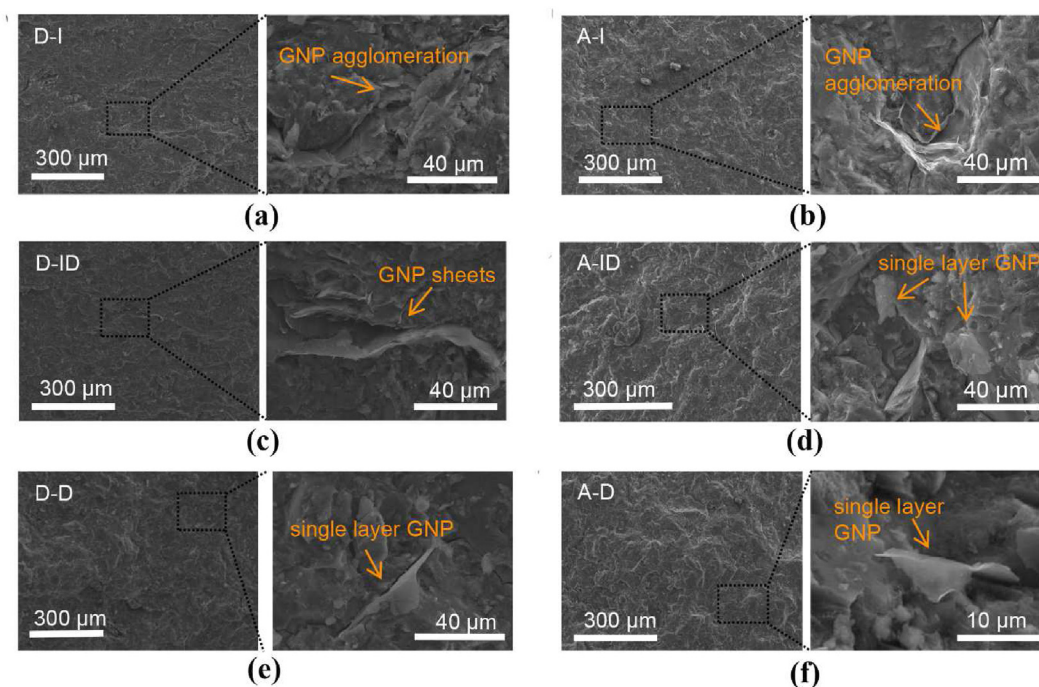


Fig. 6. SEM images of CMs with different mixing approaches: (a) direct mixing + indirect ultrasonic stirring (D-I), (b) direct mixing + combined ultrasonic stirring (D-ID), (c) direct mixing + direct ultrasonic stirring (D-D), (d) atomization mixing + indirect ultrasonic stirring (A-I), (e) atomization mixing + combined ultrasonic stirring (A-ID) and (f) atomization mixing + direct ultrasonic stirring (A-D).

gray value distribution histograms of sample A-D. The low gray values denote the low density phases that can be GNP agglomerations and pores, while the high gray values represent the high density phases that contain anhydrous cement clinkers and cement hydrations. Fig. 7c comparatively shows the cumulative volumes (containing both big pores and GNP clusters) for samples A-D and D-I. Obviously, the cumulative volumes of the low density phase of sample A-D were much smaller than those of sample D-I.

Elaborate analyses were performed to the selected regions of interest (ROIs). However, it is difficult to distinguish between the voids and GNP agglomerations with the gray value threshold, because they almost possessed the similar gray values. Therefore a further threshold method based on the geometric characteristics of the objects was used [72]. Here, the parameters of sphericity and compactness were employed. The sphericity of a pore is measured as the ratio of an ideal sphere's surface area (A_{sph}) to this pore (A_p) with the same volume (sphericity = A_{sph}/A_p), and the compactness is denoted as the ratio of the pore's volume (V_p) to its circumscribed sphere (V_{sph}) (compactness = V_p/V_{sph}) [73]. Both the sphericity and compactness measure the deviation extents of a pore body from an ideal sphere with the values between 0 and 1. A higher value of sphericity or compactness suggests the closer of the pore to the ideal sphere. Here the sphericity of 0-0.4 and compactness of 0-0.15 were set to identify GNP agglomerations (more information of the sets can be found in the supporting information Figs. S2 and S3).

2D and 3D CT images of the low density phases (including GNPs and pores) were representatively demonstrated in Fig. 7d and e. In sample D-I, many large regular and irregular objects were probed, which may be the GNP agglomeration clusters (Fig. 7f) and the entrapped air voids (Fig. 7g). Those irregular GNP agglomerations were consistent with the SEM characteristic results (Fig. 6a). Note that while the resolved air void approached a sphere, its surface was quite rough. Similar observations of air voids in CMs were reported elsewhere [65,74]. Different from the observations of sample D-I, less and small-sized platelet-like phases were found in the matrix of sample A-D (Fig. 7f) and the GNP agglomerations were much smaller (Fig. 7h). On the whole, sample A-D showed the much less GNP agglomerations in the CM matrix than sample D-I.

3.6. Pore structure

MIP was used for pore structure characterization. Generally, the pits, cavities and gaps (or size over 10 μm) on the surfaces of samples are first filled by mercury under relatively low applied pressures; later the capillary pores and gel pores formed by the growth of calcium-silicate-hydrates (CSH) are progressively occupied by mercury drops with small menisci. The progressive penetration process of MIP test enables understanding of how pores are connected to form percolation [65]. Fig. 8 shows the accumulative pore size distributions (APSDs) and differential pore size distributions (DPSDs) curves of samples A-D and D-I. Mercury first rises slightly at the beginning stage of mercury intrusion at relatively low pressures (corresponding to pore size over 100 μm). The mercury accumulations by surface irregularities that consist of voids, cracks, cavities and grain gaps can be termed as the surface conformance effect [75]. In this stage, very minor volumes of the pores over 50 nm were detected, so the spectra were not demonstrated in the figure. Two main peaks (14 nm and 21 nm) appeared in the DPSD curves of both D-I and A-D samples (Fig. 8a). Those could be the space between the packed calcium-silicate-hydrate (CSH) gels and/or the gaps between CSH particles and GNP sheets. Both pore peak intensities and APSD spectra intensities of D-I were higher than those of A-D (Fig. 8b), suggesting that the A-D method would cause denser CSH compactness and less GNP agglomerations. As a result, the total porosity decreased from 0.143 (D-I sample) to 0.113 (A-D sample) by 21% and the density increased from 1.883 g/cm^3 (D-I sample) to 2.045 g/cm^3 (A-D sample) by 8.6%, respectively. The pore data strongly evidenced that the hybrid ultrasonic stirring and atomization approach can efficiently eliminate the pores in cement matrix as well as the defects between cement hydrates and GNP sheets. The results of MIP are also in line with those of SEM and XCT (Figs. 6 and 7).

3.7. Chemical outcomes

Results of chemical tests for samples D-I, A-D and Ref. are displayed in Fig. 9. TG/DTG spectra for these samples cured for 1d and 28d are shown

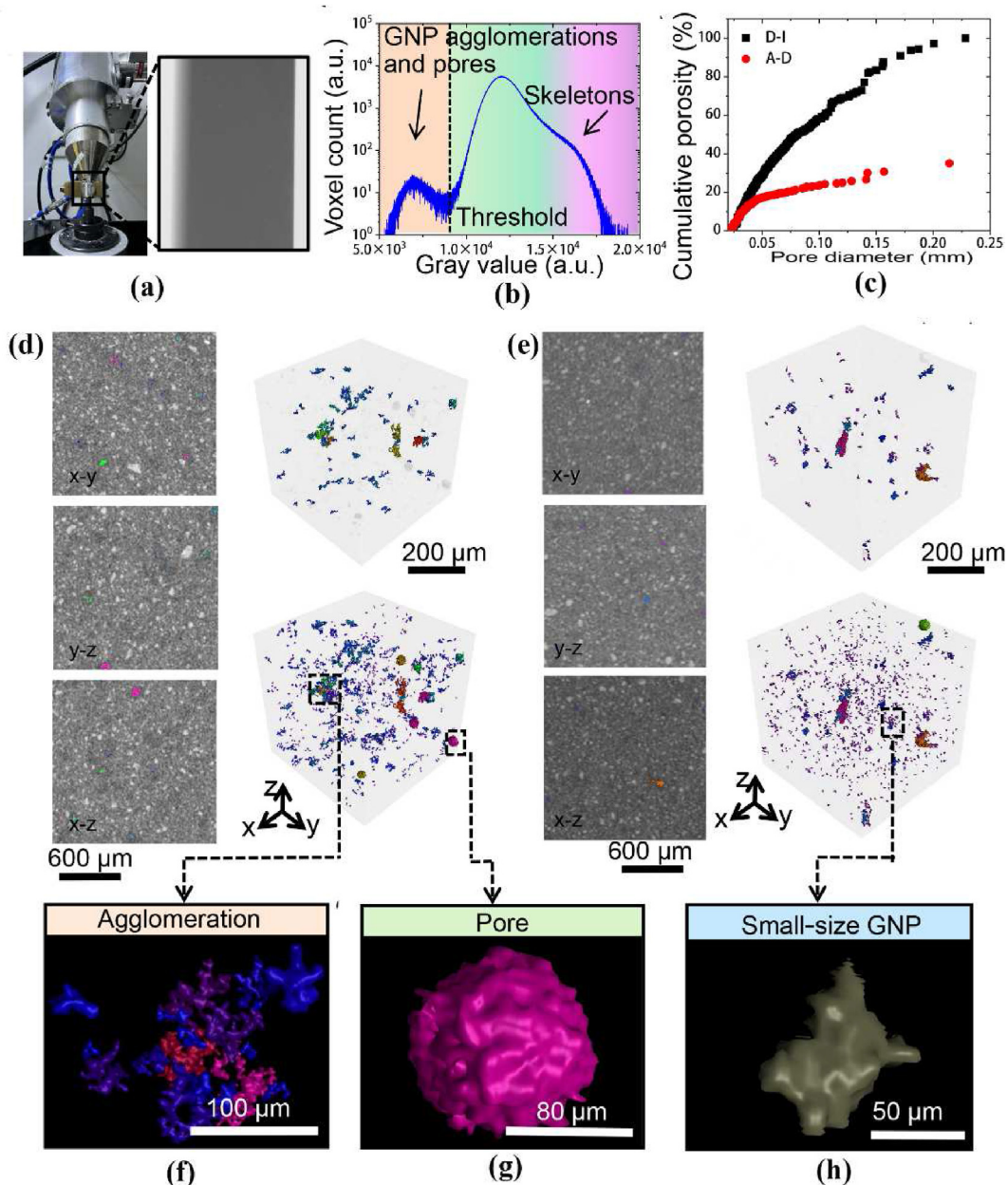


Fig. 7. XCT tests and results of samples A-D and D-I: (a) XCT scans of a sample, (b) phase recognition with gray value threshold of sample A-D, (c) comparative plots of cumulative porosity; phase reconstruction of (d) sample D-I and (e) sample A-D, as well as the local structure of (f) large GNP agglomeration clusters in sample D-I, (g) a big void in sample D-I, and (h) very small GNP agglomeration in sample A-D.

in Fig. 9a and b. Three obvious mass-loss phases were identified in the figure. The mass loss below 150 °C is caused by the desorption/evaporation of the water that has been initially and physically confined in thin pores (and/or bonded with pore walls) and the dehydration of some crystals such as ettringite and gypsum [76]. The second obvious mass loss that occurred at around 450 °C represents the decomposition of CH, which accounts for nearly 6% of the total mass, so a sharp downward peak in the DTG spectra was observed. The mass loss peak at around 625 °C is assigned to the decomposition of calcium carbonate that may be caused by the carbonation of cement hydrates under ambient environments [14].

As can be seen in Fig. 9a and b, the TG curves of the three samples almost were superimposed together, suggesting that they possessed no great differences in hydration products at 1 d. At 28, however, the mass losses were greatly increased due to the continual hydration of cement clinkers. The extents of mass loss ascended in order of samples Ref., D-I

and A-D. This implied that regardless of the mixing methods, the incorporation of GNPs or other CNAs into cement can always enhance cement hydration [77]. The TG/DTG data testified that the A-D scheme had the largest impacts on cement hydration.

Fig. 9c shows the FTIR spectra of the GNP-modified CM samples. The band around 3645 cm^{-1} indicates the vibrations of -OH in CH, while the broad peak at 3440 cm^{-1} denotes the stretching vibration of -OH in free or confined water [78]. The peak at 1600 cm^{-1} represents the vibrations of H-O-H bend from the physically absorbed and confined water. It also shows the characteristic peak of C-O stretching from CaCO_3 at 1450 cm^{-1} [79]. The peaks around 1000 cm^{-1} indicate the stretching vibrations of Si-O in CSH. It seems that the Si-O stretching vibrations in sample A-D were higher than those in samples D-I and Ref., again, suggesting that the proposed hybrid ultrasonic stirring and atomization mixing scheme can enhance cement hydration. Similar findings were reported elsewhere [80].

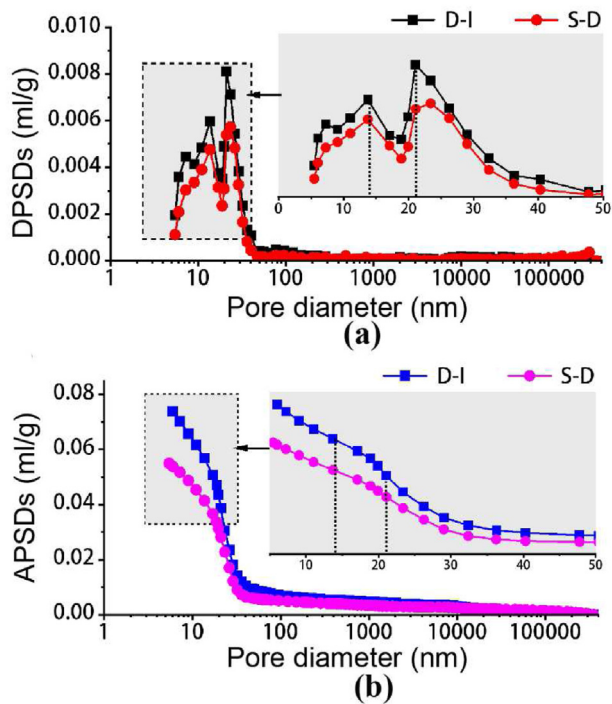


Fig. 8. MIP pore structure: (a) DPDSs and (b) APDSs curves of samples D-I and A-D.

Fig. 9d shows the XRD patterns of the GNP-modified CM samples. Several representative hydration phases, i.e., CH, ettringite (Aft), and anhydrous phases such as Alite and Belite can be depicted in the samples according to their XRD characteristics [81]. The hydration products showed higher XRD characteristic peak intensities, while the anhydrous

phases displayed lower ones for the samples with longer curing ages (Fig. 9d). This evidenced the continual consumption of the anhydrous clinkers and the formation of the hydration products with time [82]. At the same curing age, the intensity of CH and Aft of D-I and A-D were higher than those in the Ref. sample, again evidencing the acceleration effect of GNPs on cement hydration [83]. The hydration acceleration effect of GNPs as well as other CNAs may involve both physical and chemical issues. On one hand, the nano sized GNPs can fill the space between cement particles, and their high surface areas can provide additional sites for the nucleation of hydration products [65]. On the other hand, the functional groups on GNPs may adsorb Ca^{2+} , which would be beneficial to the dissolution of cement clinkers [83].

Overall, the chemical outcomes from TG/DTG, FTIR and XRD tests proved that: 1) incorporation of nano materials like GNPs into cement can always promote cement hydration regardless of the stirring and mixing schemes, and 2) the atomization approach (A-D) had the largest acceleration effect on cement hydration. The chemical outcomes (Fig. 9) together with the results of microstructure, GNP agglomeration, and pore structure (Figs. 6–8) evidently proved the densest material compactness and highest compressive strength promotion of GNPs modified CMs (Fig. 5) fabricated with the proposed atomization dispersion approach.

4. Conclusions

In this work, we developed a simple dispersion approach by integrating ultrasonication and atomization in a home-made automatic devices. Microscopy and UV-Vis tests showed that the direct ultrasonic stirrings can efficiently disperse GNPs and maintain the dispersion status. The atomization process generated massive small droplets with a characteristic size around $100 \mu\text{m}$, which prevents the GNPs from serious agglomerations. Tests on the GNP-modified CMs demonstrated that monolayer GNP sheets were observed in the materials with the A-D approach, while severe agglomerations occurred in the materials with the ordinary mixing process. At the optimal GNP dosage (0.3 wt% to

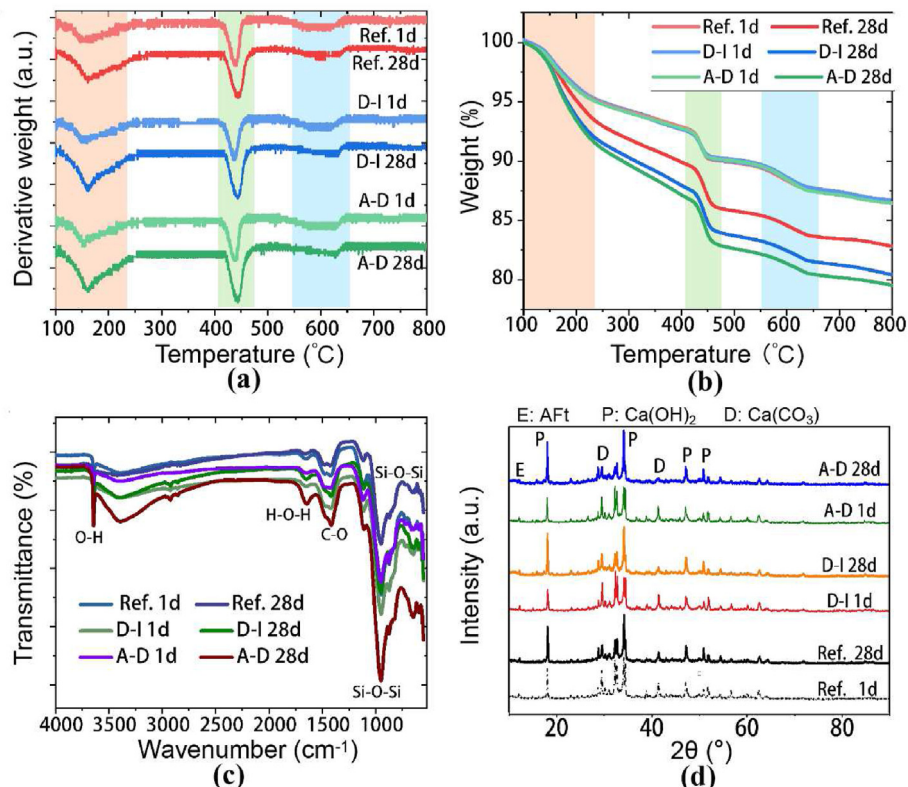


Fig. 9. Chemical outcomes: (a) DTG and (b) TG spectra, (c) FTIR spectra and (d) XRD patterns of the Ref., D-I, and A-D samples at 1 d and 28 d.

cement), the compressive strength of the A-D sample was raised by 54% when compared with the Ref. sample, much higher than the data documented. Large GNP agglomeration clusters were detected by XCT for the sample without the A-D approach. The total porosity of the A-D sample was 21% lower than that of the D-I sample. Furthermore, the A-D approach also accelerated cement hydration according to the chemical tests results, ascribed to the filling effects and the excess surface areas for nucleation. In light of all the findings in this study, the hybrid ultrasonic stirring and atomization approach offers an effective method to disperse GNPs and other nano fillers into engineering materials. In industrialization aspects, the devices for atomization and ultrasonication are highly available and rather cheap, it thus can be expected that this approach can be easily employed industrial utilization without large R&D costs.

CRedit author statement

Nanxi Dang: Methodology, Software, Writing- Original draft preparation. Rijiao Yang: Methodology, Software. Chengji Xu: Methodology, Software. Peng Yu: Methodology, Software. Qiang Zeng: Conceptualization, Writing- Reviewing and Editing, Supervision. Weijian Zhao: Conceptualization, Writing- Reviewing and Editing, Supervision. Zhidong Zhang: Methodology, Supervision.

Data availability

Data will be made available on request.

Declaration of competing interest

The authors declare that they have no known competing financial interests or personal relationships that could have appeared to influence the work reported in this paper.

Acknowledgments

The research was supported by the Fundamental Research Funds for the Central Universities (No. 226-2023-00010), National Natural Science Foundation of China (No. 52038004) and ZJU-ZCCC Institute of Collaborative Innovation (No. ZDJG2021008).

Appendix A. Supplementary data

Supplementary data to this article can be found online at <https://doi.org/10.1016/j.nanoms.2023.09.004>.

References

- [1] A. Osman, A. Elhakeem, S. Kaytbay, A. Ahmed, A comprehensive review on the thermal, electrical, and mechanical properties of graphene-based multi-functional epoxy composites, *Adv. Compos. Hybrid Mater.* 5 (2022) 547–605.
- [2] X. Duan, S. Cheng, R. Tao, Z. Zhang, G. Zhao, Synergistically enhanced thermal conduct ability and mechanical properties of natural rubber for tires through a graphene/silica with a dot-face structure, *Adv. Compos. Hybrid Mater.* 5 (2022) 1145–1157.
- [3] C. Vallés, X. Zhang, J. Cao, F. Lin, R. Young, A. Lombardo, A. Ferrari, L. Burk, R. Mulhaupt, I. Kinloch, Graphene/polyelectrolyte layer-by-layer coatings for electromagnetic interference shielding, *ACS. Appl. Mater.* 2 (2019) 5272–5281.
- [4] X. Su, R. Wang, X. Li, S. Araby, H. Kuan, M. Naeem, J. M, A comparative study of polymer nanocomposites containing multi-walled carbon nanotubes and graphene nanoplatelets, *Nano. Mater. Sci.* 4 (2022) 185–204.
- [5] M. Wang, M. Huang, D. Luo, Y. Li, M. Choe, W. Seong, M. Kim, S. Jin, M. Wang, R. Ruoff, Single-crystal, large-area, fold-free monolayer graphene, *Nature* 596 (2021) 519–524.
- [6] G. Fan, Z. Wang, K. Sun, Y. Liu, R. Fan, Doped ceramics of indium oxides for negative permittivity materials in MHz-kHz frequency regions, *J. Mater. Sci. Technol.* 61 (2021) 125–131.
- [7] Z. Zhang, M. Liu, M. Ibrahim, H. Wu, Y. Wu, Y. Li, G.M. Mersal, I. El Azab, S. El-Bahy, M. Huang, Y. Jiang, G. Liang, P. Liu C, Flexible polystyrene/graphene composites with epsilon-near-zero properties, *Adv. Compos. Hybrid Mater.* 5 (2022) 1054–1066.
- [8] P. Xie, Z. Shi, M. Feng, K. Sun, Y. Liu, K. Yan, C. Liu, T. Moussa, M. Huang, S. Meng, G. Liang, H. Hou, R. Fan, Z. Guo, Recent advances in radio-frequency negative

- dielectric metamaterials by designing heterogeneous composites, *Adv. Compos. Hybrid Mater.* 5 (2022) 679–695.
- [9] M. Liu, H. Wu, Y. Wu, P. Xie, R. Pashameah, H. Abo-Dief, S. El-Bahy, Y. Wei, G. Li, W. Li, G. Liang, C. Liu, K. Sun, R. Fan, The weakly negative permittivity with low-frequency-dispersion behavior in percolative carbon nanotubes/epoxy nanocomposites at radio-frequency range, *Adv. Compos. Hybrid Mater.* 5 (2022) 2021–2030.
- [10] M. Song, J. Wang, L. Yuan, C. Luan, Z. Zhou, Investigation on crack recovery behavior of engineered cementitious composite (ECC) incorporated memory alloy fiber at low temperature, *ES Materials & Manufacturing* (2022) 17 23–33.
- [11] R. He, T. Nantung, J. Olek, N. Lu, Use of Dielectric Constant for Determination of Water-To-Cement Ratio (W/C) in Plastic Concrete: Part 2: Comparison Determined W/C Values by Ground Penetrating Radar (GPR) and Microwave Oven Drying Measurements, 2023.
- [12] C. Jing, B. Dong, A. Raza, T. Zhang, Y. Zhang, Corrosion inhibition of layered double hydroxides for metal-based systems, *Nano. Mater. Sci.* 3 (2021) 47–67.
- [13] W. Dong, W. Li, Z. Sun, I. Ibrahim, D. Sheng, Intrinsic graphene/cement-based sensors with piezoresistivity and superhydrophobicity capacities for smart concrete infrastructure, *Autom. Construct.* 133 (2022) 103983.
- [14] L. Lavagna, D. Massella, E. Priola, M. Pavese, Relationship between oxygen content of graphene and mechanical properties of cement-based composites, *Cem. Concr. Compos.* 115 (2021) 103851.
- [15] B. Wang, D. Shuang, Effect of graphene nanoplatelets on the properties, pore structure and microstructure of cement composites, *Mater. Express* 8 (2018) 407–416.
- [16] M. Law, Y. Zhao, W. Zhang, R. Wang, M. Shi, Y. Zhang, J. Yang, Highly transparent and super-wettable nanocoatings hybridized with isocyanate-silane modified surfactant for multifunctional applications, *Nano. Mater. Sci.* 4 (2022) 151–168.
- [17] P. Dalla, I. Tragazikis, G. Trakakis, C. Galiotis, K. Dassios, T. Matikas, Multifunctional cement mortars enhanced with graphene nanoplatelets and carbon nanotubes, *Sensors* 21 (2021) 933.
- [18] Y. Yao, Z. Zhang, H. Liu, Y. Zhuge, D. Zhang, A new in-situ growth strategy to achieve high performance graphene-based cement material, *Construct. Build. Mater.* 335 (2022) 127451.
- [19] B. Wang, R. Jiang, Z. Wu, Investigation of the mechanical properties and microstructure of graphene nanoplatelet-cement composite, *Nanomaterials* 6 (2016) 200.
- [20] M. Di Mare, N. Inumerable, P. Brisebois, C. Ouellet-Plamondon, Combined experimental and computational prediction of the piezoresistivity of alkali-activated inorganic polymers, *J. Phys. Chem. C* 126 (2022) 14995–15000.
- [21] Z. Zhou, H. Zhang, J. Qiu, P. Chen, W. Sun, Atomic insights into synergistic effect of pillared graphene by carbon nanotube on the mechanical properties of polymer nanocomposites, *Nano. Mater. Sci.* 4 (2022) 235–243.
- [22] G. Jing, H. Feng, Q. Li, X. Li, J. Wu, S. Wang, Z. Ye, Enhanced dispersion of graphene oxide in cement matrix with isolated-dispersion strategy, *Ind. Eng. Chem. Res.* 59 (2022) 10221–10228.
- [23] X. Zhu, X. Kang, Effect of graphene oxide (GO) on the hydration and dissolution of the elite in a synthetic cement system, *J. Mater. Sci.* 55 (2022) 3419–3433.
- [24] A. Mehmood, N. Mubarak, M. Khalid, R. Walvekar, E. Abdullah, M. Siddiqui, H. Baloch, S. Nizamuddin, S. Mazari, Graphene-based nanomaterials for strain sensor application A-review, *J. Environ. Chem. Eng.* 8 (2020) 103743.
- [25] S. Ding, Y. Xiang, Y. Ni, V.K. Thakur, X. Wang, B. Han, J. Ou, In-situ synthesizing carbon nanotubes on cement to develop self-sensing cementitious composites for smart high-speed rail infrastructures, *Nano Today* 43 (2022) 101438.
- [26] E. Polonina, V. Potapov, S. Zhdanok, S. Leonovich, Mechanism for improving the strength of a cement material modified by SiO₂ nanoparticles and multiwall carbon nanotubes, *J. Eng. Phys. Thermophys.* 94 (2021) 67–78.
- [27] Y. Wang, R. Li, T. Yuan, Microstructure and mechanical properties of Al-Si-Ni coating on Cu-Cr substrate prepared by multi-permeation and friction stir processing, *Nano. Mater. Sci.* 1 (2019) 224–228.
- [28] X. Wang, D. Feng, J. Zhong, X. Shi, Reinforcement of cement paste by reduced graphene oxide: effect of dispersion state, *Mater. Struct.* 55 (2022) 25.
- [29] H. Du, H. Gao, S. Pang, Improvement in concrete resistance against water and chloride ingress by adding graphene nanoplatelet, *Cement Concr. Res.* 83 (2016) 114–123.
- [30] J. Liu, H. Suh, H. Jee, J. Xu, E.Z. Nezhad, C.S. Choi, S. Bae, Synergistic effect of carbon nanotube/TiO₂ nanotube multi-scale reinforcement on the mechanical properties and hydration process of portland cement paste, *Construct. Build. Mater.* 293 (2021) 123447.
- [31] B. Wang, Y. Han, S. Liu, Effect of highly dispersed carbon nanotubes on the flexural toughness of cement-based composites, *Construct. Build. Mater.* 46 (2013) 8–12.
- [32] A. Sobolkina, V. Mechtcherine, V. Khavrus, D. Maier, M. Mende, M. Ritschel, A. Leonhardt, Dispersion of carbon nanotubes and its influence on the mechanical properties of the cement matrix, *Cem. Concr. Compos.* 34 (2012) 1104–1113.
- [33] S. Bai, L. Jiang, N. Xu, M. Jin, S. Jiang, Enhancement of mechanical and electrical properties of graphene/cement composites due to improved dispersion of graphene by addition of silica fume, *Construct. Build. Mater.* 164 (2018) 433–441.
- [34] S. Yaseen, G. Yiseen, Z. Li, Elucidation of calcite structure of calcium carbonate formation based on hydrated cement mixed with graphene oxide and reduced graphene oxide, *ACS Omega* 4 (2019) 10160–10170.
- [35] T. Qureshi, D. Panesar, Nano reinforced cement paste composite with functionalized graphene and pristine graphene nanoplatelets, *Compos. B Eng.* 197 (2020) 108063.
- [36] J. Tao, X. Wang, Z. Wang, Q. Zeng, Graphene nanoplatelets as an effective additive to tune the microstructures and piezoresistive properties of cement-based composites, *Construct. Build. Mater.* 209 (2019) 665–678.

- [37] X. Li, L. Wang, Y. Liu, W. Li, B. Dong, W.H. Duan, Dispersion of graphene oxide agglomerates in cement paste and its effects on electrical resistivity and flexural strength, *Cem. Concr. Compos.* 92 (2018) 145–154.
- [38] Z. Lu, D. Hou, A. Hanif, W. Hao, Z. Li, G. Sun, Comparative evaluation on the dispersion and stability of graphene oxide in water and cement pore solution by incorporating silica fume, *Cem. Concr. Compos.* 94 (2018) 33–42.
- [39] C. Ruan, J. Lin, S. Chen, K. Sagoe-Crentsil, W. Duan, Effect of graphene oxide on the pore structure of cement paste: implications for performance enhancement, *ACS Appl. Nano Mater.* 4 (2021) 10623–10633.
- [40] B. Zhang, T. Chen, Study of ultrasonic dispersion of graphene nanoplatelets, *Materials* 12 (2019) 1757.
- [41] K. Muthoosamy, S. Manickam, State of the art and recent advances in the ultrasonic-assisted synthesis, exfoliation, and functionalization of graphene derivatives, *Ultrason. Sonochem.* 39 (2017) 478–493.
- [42] J. Liu, J. Fu, Y. Yang, C. Gu, Study on dispersion, mechanical and microstructure properties of cement paste incorporating graphene sheets, *Construct. Build. Mater.* 199 (2019) 1–11.
- [43] H. Du, S. Pang, Dispersion and stability of graphene nanoplatelet in water and its influence on cement composites, *Construct. Build. Mater.* 167 (2018) 403–413.
- [44] M. Konsta-Gdoutos, Z. Smetaxa, S. Shah, Highly dispersed carbon nanotube reinforced cement-based materials, *Cement Concr. Res.* 40 (2010) 1052–1059.
- [45] I. Papanikolaou, L. de Souza, C. Litina, A. Al-Tabbaa, Investigation of the dispersion of multi-layer graphene nanoplatelets in cement composites using different superplasticiser treatments, *Construct. Build. Mater.* 293 (2021) 123543.
- [46] F. Ghaharpour, A. Bahari, M.A. Abbasi, A. Ashkarran, Parametric investigation of CNT deposition on cement by CVD process, *Construct. Build. Mater.* 113 (2016) 523–535.
- [47] L. Nasibulina, I. Anoshkin, S. Shandakov, A. Nasibulin, A. Cwirzen, R. Mudimela, K. Habermehl-Cwirzen, J. Malm, T.S. Koltsova, Y. Tian, Direct synthesis of carbon nanofibers on cement particles, *Transport. Res. Rec.* 2142 (2010) 96–101.
- [48] A. Al-Dahawi, O. Öztürk, F. Emami, G. Yıldırım, M. Şahmaran, Effect of mixing methods on the electrical properties of cementitious composites incorporating different carbon-based materials, *Construct. Build. Mater.* 104 (2016) 160–168.
- [49] D. Ng, S. Paul, V. Anggraini, S. Kong, T. Qureshi, C. Rodriguez, B. Šavija, Influence of SiO₂, TiO₂ and Fe₂O₃ nanoparticles on the properties of fly ash blended cement mortars, *Construct. Build. Mater.* 258 (2020) 119627.
- [50] O. Ozbulut, Z. Jiang, D. Harris, Exploring scalable fabrication of self-sensing cementitious composites with graphene nanoplatelets, *Smart Mater. Struct.* 27 (2018) 115029.
- [51] S. Alla, S. Asadi, Investigation on fluidity, microstructure, mechanical and durability properties of snail shell based graphene oxide cement composite material, *Construct. Build. Mater.* 362 (2023) 129767.
- [52] D. Lu, Z. Leng, G. Lu, D. Wang, Y. Huo, A critical review of carbon materials engineered electrically conductive cement concrete and its potential applications, *Int. J. Soc. Netw. Min.* (2023) 1–27.
- [53] C. Liu, X. Huang, Y. Wu, X. Deng, Z. Zheng, Z. Xu, D. Hui, Advance on the dispersion treatment of graphene oxide and the graphene oxide modified cement-based materials, *Nanotechnol. Rev.* 10 (2021) 34–49.
- [54] Z. Lu, D. Hou, A. Hanif, W. Hao, Z. Li, G. Sun, Comparative evaluation on the dispersion and stability of graphene oxide in water and cement pore solution by incorporating silica fume, *Cem. Concr. Compos.* 94 (2018) 33–42.
- [55] S. Ghazizadeh, P. Duffour, N. Skipper, M. Billing, Y. Bai, An investigation into the colloidal stability of graphene oxide nano-layers in alite paste, *Cement Concr. Res.* 99 (2017) 116–128.
- [56] H. Zhu, K. Yu, V. Li, Sprayable engineered cementitious composites (ECC) using calcined clay limestone cement (LC3) and PP fiber, *Cem. Concr. Compos.* 115 (2021) 103868.
- [57] L. Chen, P. Li, G. Liu, W. Cheng, Z. Liu, Development of cement dust suppression technology during shotcrete in mine of China-A review, *J. Loss Prev. Process. Ind.* 55 (2018) 232–242.
- [58] C. Herrera-Mesen, R. Salvador, T. Ikumi, S. Cavalaro, A. Aguado, External sulphate attack of sprayed mortars with sulphate-resisting cement: influence of accelerator and age of exposition, *Cem. Concr. Compos.* 114 (2020) 103614.
- [59] E. Hartono, A. Muntohar, N. Abiyoga, Influence of the pulverised method on the plasticity and strength behaviour of cement stabilised clay shale and sandstone, *Mater. Sci. Eng.* 1144 (2021) 012096.
- [60] L. Li, D. Xuan, S. Chu, J. Lu, C. Poon, Efficiency and mechanism of nano-silica pre-spraying treatment in performance enhancement of recycled aggregate concrete, *Construct. Build. Mater.* 301 (2021) 124093.
- [61] S. Papatzani, Effect of nanosilica and montmorillonite nanoclay particles on cement hydration and microstructure, *Mater. Sci. Technol.* 32 (2) (2016) 138–153.
- [62] B. Liu, X. Lu, H. Meng, G. Pan, D. Li, Dispersion of in-situ controllably grown nano-SiO₂ in alkaline environment for improving cement paste, *Construct. Build. Mater.* 369 (2023) 130460.
- [63] S. Mandal, A. Sadeghianjahromi, C. Wang, Experimental and Numerical Investigations on Molten Metal Atomization Techniques-A Critical Review, 33, 2022 103809, 11.
- [64] W. Dong, W. Li, Y. Guo, K. Wang, D. Sheng, Mechanical properties and piezoresistive performances of intrinsic graphene nanoplate/cement-based sensors subjected to impact load, *Construct. Build. Mater.* 327 (2022) 126978.
- [65] Q. Zeng, S. Chen, P. Yang, Y. Peng, J. Wang, C. Zhou, D. Yan, Reassessment of mercury intrusion porosimetry for characterizing the pore structure of cement-based porous materials by monitoring the mercury entrapments with X-ray computed tomography, *Cem. Concr. Compos.* 113 (2020) 103726.
- [66] X. Xi, Q. Shi, S. Jiang, K. Wang, Z. Wu, H. Shao, Effects of graphene oxide on the mechanical and microscopic characteristics of cement-based plugging material for preventing spontaneous combustion of coal, *Energy Fuels* 34 (2020) 6346–6354.
- [67] Y. Wang, J. Xu, Y. Liang, H. Yin, W. Long, P. Pu, J. Liu, PDMS/CNB-impregnation treatment for improving the electrical and piezoresistive properties of recycled fine aggregate mortar, *J. Build. Eng.* (2023) 106253.
- [68] G. Xiong, Y. Ren, C. Wang, Z. Zhang, S. Zhou, C. Kuang, S. Hong, Effect of power ultrasound assisted mixing on graphene oxide in cement paste: dispersion, microstructure and mechanical properties, *J. Build. Eng.* (2023) 106321.
- [69] F. Wang, M. Hao, W. Liu, P. Yan, B. Fang, S. Li, L. Cui, Low-cost fabrication of highly dispersed atomically-thin MoS₂ nanosheets with abundant active Mo-terminated edges, *Nano Mater. Sci.* 3 (2021) 205–212.
- [70] Y. Sheng, C. Zhu, A. Abdulakeem, P. Hu, Z. Ye, L. Wang, L. Li, Study on mechanical properties of graphene modified cement mortar, Fullerenes, Nanotub. Carbon Nanostruct. (2022) 1–16.
- [71] M. Krystek, A. Ciesielski, P. Samori, Graphene-based cementitious composites: toward next-generation construction technologies, *Adv. Funct. Mater.* 31 (2021) 2101887.
- [72] G. Jing, H. Feng, Q. Li, X. Li, J. Wu, S. Wang, Z. Ye, Enhanced dispersion of graphene oxide in cement matrix with isolated-dispersion strategy, *Ind. Eng. Chem. Res.* 59 (2020) 10221–10228.
- [73] Y. Peng, G. Zhao, Y. Qi, Q. Zeng, In-situ Assessment of the Water-Permeation Resistance of Polymer Modified Cement Mortars by μ -XCT, SEM and EDS, *Cem Concr Compos.* 2020 103821.
- [74] X. Wang, Y. Peng, J. Wang, Q. Zeng, Pore structure damages in cement-based materials by mercury intrusion: a non-destructive assessment by X-ray computed tomography, *Materials* 12 (2019) 2220.
- [75] J. Wang, J. Tao, L. Li, C. Zhou, Q. Zeng, Thinner fillers, coarser pores? A comparative study of the pore structure alterations of cement composites by graphene oxides and graphene nanoplatelets, *Composites part A* 130 (2020) 105750.
- [76] T. Gu, Y. Zheng, H. Yue, Y. Zheng, Characterization of the pore structure of well cement under carbon capture and storage conditions by an image-based method with a combination of metal intrusion, *ACS Omega* 6 (2021) 2110–2120.
- [77] A. Ahmad, M. Sutanto, N. Ahmad, M. Mohamad, M. Bujang, Microstructural characterization of fibric peat stabilized with portland cement and silica fume, *Materials* 16 (2023) 18.
- [78] Z. Metaxa, S. Boutsoukou, M. Amenta, E. Favvas, S. Kourkoulis, N. Alexopoulos, Dispersion of multi-walled carbon nanotubes into white cement mortars: the effect of concentration and surfactants, *Nanomaterials* 12 (2022) 1031.
- [79] J. Wang, J. Tao, L. Li, C. Zhou, Q. Zeng, Thinner fillers, coarser pores? A comparative study of the pore structure alterations of cement composites by graphene oxides and graphene nanoplatelets, *Composites Part A* 130 (2020) 105750.
- [80] G. Mishra, Co-effect of carbon nanotube and nano-sized silica on dispersion and mechanical performance in cementitious system, *Diam. Relat. Mater.* (2022) 109162.
- [81] N. Bossa, P. Chaurand, J. Vicente, D. Borschneck, C. Levard, O. Aguerre-Chariol, J. Rose, Micro- and nano-X-ray computed-tomography: a step forward in the characterization of the pore network of a leached cement paste, *Cement Concr. Res.* 67 (2015) 138–147.
- [82] C. Xu, Y. Dai, Y. Peng, J. Wang, Z. Zhang, Q. Gui, Q. Zeng, Multi-scale structure of in-situ polymerized cementitious composites with improved flowability, strength, deformability and anti-permeability, *Compos. B Eng.* 245 (2022) 110222.
- [83] F. Pang, C. Wei, Z. Zhang, W. Wang, Z. Wang, The migration and immobilization for heavy metal chromium ions in the hydration products of calcium sulfoaluminate cement and their leaching behavior, *J. Clean. Prod.* 365 (2022) 132778.